Iranian Journal of Analytical Chemistry
Volume 11, Issue 1, March 2024 (30-43) Original Research Article

مجله ایرانی شیمی تجزیه
دوره ۱۱، شماره ۱، فروردین۱۴۰۳ (۴۳-۳۰)

Adsorptive Removal of Pb(II) Ions by Using Multiwall Carbon Nanotube/ZnCo- Zeolite Imidazole Frameworks: Optimization and Modelling Study

Sayed Zia Mohammadi[1*], Sareh Torabian[1], Somayeh Tajik[2]

1-Department of Chemistry, Payame Noor University, Tehran, Iran
2- Research Center of Tropical and Infectious Diseases, Kerman University of Medical Sciences, P.O. Box 76169-13555, Kerman, Iran

Received: 14 July 2024 **Accepted:** 8 August 2024
DOI: 10.30473/ijac.2024.71788.1303

Abstract
In the present research, an effective adsorbent as titled multiwall carbon nanotube/ZnCo- Zeolite imidazole frameworks (MWC/ZIF) was prepared and used for removal of Pb(II) ion from effluent samples. After separating the adsorbent from the solution, the amount of Pb(II) ion in the solution was measured using an atomic absorption device. Based on this, various experimental parameters effective on lead removal including pH, ionic strength, time, temperature, and Pb(II) ion concentration were investigated. Various kinetic models were also studied to assess adsorption kinetics of Pb(II) ions onto surface of MWC/ZIF nanocomposite. With reference to the obtained findings, the produced nanocomposite was assumed as an effective adsorption approach for removal of Pb(II) ions from effluent samples.

Keywords
Multiwall carbon nanotube; ZnCo- Zeolite imidazole frameworks; Pb(II) ion; Removal; Nanocomposite.

1.INTRODUCTION

Recently, due to the rapid rate of industrial development and urbanization, the existing water sources have been polluted by heavy metal ions such as nickel, zinc, copper, cadmium and lead. Unfortunately, these pollutions are increased due to discharge of effluent from various factories into the environment. [1-3]. When these toxic ions enter the environment, they are not decomposed and enter the human body through the food chain and accumulate in it, causing serious health problems such as the brain, liver, kidneys, and lungs [1,4,5]. Lead is a widely used metal and used in many industries such as battery making, metal finishing, painting and ammunition making, and therefore it is present in the effluent of these factories and if these effluents enters the environment without pre-treatment and purification, could cause many problems for human health [6]. Lead ion accumulates in different body tissues therefore, human contact with contaminated sources of lead even in low concentrations can cause problems in adults such as memory loss, biological disorders and serious damage to the kidney and nervous systems [4,5]. Poisoning of children with lead can cause many problems, such as serious damage to the brain and nervous system, learning problems and reduced growth [6,7].

So far, different methods were used for the elimination of lead ions from water specimen, including precipitation, coprecipitation, ion exchange, flotation membranes, chemical precipitation, electrochemical treatment, ultrafiltration, desalination, filtration, biosorption, membrane filtration, extraction and adsorption [6-14]. Among these methods, the adsorption method has been widely used by all researchers due to its simplicity, cheapness, variety of adsorbents and high efficiency [1,15,16]. The type of absorbent used in absorption methods is very important and effective. Various types of adsorbents have been used by researchers to remove lead ions such as Chitosan cross-linked and grafted with epichlorohydrin and 2,4-dichlorobenzaldehyde [1], modified activated carbon by amine and thiol [17], activated carbon[18,19], polyacrylic acid capped Fe_3O_4 – Cu-MOF [20], ninhydrin-functionalized chitosan [21], Low cost bio-sorbent derivated from Melon Peel [22], the modified

* Corresponding author:
S. Z.Mohammadi; E-mail: szmohammadi@pnu.ac.ir

Cassia fistula seeds [23], Co3O4@SiO2 magnetic nanoparticle-nylon 6 [24], magnetic nanoparticles-embedded nitrogen-doped carbon nanotube/porous carbon hybrid [25], Graphene oxide decorated with fullerenol nanoparticles [26], green algae (spirogyra) supported with treated NaOH- rice husk ash [27], calcium oxide nanoparticles [28], modified powdered peanut shells as a bio-sorbent [29], magnetic activated carbon–cobalt nanoparticles [30] and so on.

Among the physical adsorbents, carbon based porous materials such as multiwalled carbon nanotubes (MWC) hold the greatest potential for commercial use, due to its properties such as excellent electrical conductivity, high surface area and excellent stability, in the last decades used in various fields such as nanotechnology, the design of various sensors and adsorption [31]. Further, another class of porous materials are metal organic frameworks (MOFs). MOFs are flexible crystalline solids that composed from organic ligands and metal links. The MOFs have diverse and very attractive structures due to having adjustable and completely regular pores, which has made them have various applications in different fields such as sensors, catalysis, energy storage, absorption, etc [32,33]. Zeolitic imidazolate frameworks (ZIFs) are a subset of MOFs that have imidazole bridges with metal nodes (such as Zn, Co) that have a cage-like structure similar to zeolites. The unique properties of ZIFs, such as permanent porosity and unique thermal and chemical stability, have made these materials unique candidates for attractive applications such as catalysis, separation, gas absorption/storage, and etc [31, 34,35].

ZIFs have been investigated for the preparation of porous carbon/metal oxides due to their porous structures [34]. Therefore, in the present work, we intend to combine the excellent and unique properties of MWC and ZIFs and provide a new adsorbent as titled multiwall carbon nanotube/ZnCo- Zeolite imidazole frameworks (MWC/ZIF) for the removal of Pb(II) ions from environmental samples.

2.EXPERIMENTAL

2.1. Instruments and materials

SensAA GBC atomic adsorption spectrometer (FAAS) manufactured by Dandenong Ltd. (Australia) was used for measuring absorbance of Pb with regard to the manufacturer's guidelines. Pb hollow cathode lamp was applied at wavelength of 217 nm. The pH all solutions were adjusted by using a Metrohm (Herisau, Switzerland) pH-meter model 692. All solutions were agitated by IKA stirrer model KS (Staufen; Germany).

A stock solution of Pb(II) ion (1000.0 mg L^{-1}) was prepared from Merck Co.; Darmstadt (Germany). The other solutions with low concentrations were prepared by serial dilutions of initial Pb(II) ion. Milli-Q water purifier manufactured by EMD Millipore Co. was used for production of deionized water. MWCNTs-COOH with a purity higher than 95% was purchased from US-nano Co. N-hexyl-3-methylimidazolium hexafluorophosphate with a purity higher than 97%, sodium hydroxide 98%, polyvinylpyrrolidone (PVP) 99%, methanol 99%, $Zn(NO_3)_2.6H_2O$ 98%, $Co(NO_3)_2.6H_2O$ with a purity higher than 98% and 2-methylimidazole (2-MeIm) with a purity higher than 99% were prepared from Sigma-Aldrich or Merck Co.

2.2. Synthesis of MWC/ZIF nanocomposite

The MWC/ZIF was synthesized according to the previously published article with a little modification [31]. For this purpose, 30 mL of methanol was transferred to an Erlenmeyer and polyvinylpyrrolidone (PVP) (0.35 g) and carboxylic acid functionalized MWC (0.07 g) were added to it and ultrasonicated (30 min). Then, $Zn(NO_3)_2.6H_2O$ (1.026 g) and $Co(NO_3)_2.6H_2O$ (0.996 g) were added to this mixture and stirred at room temperature (60 min). In another beaker, 30 mL methanol was poured and 2-MeIm (1.53 g) was added to it, and then the resulting solution was added dropwise to the previous solution and stirred slowly at room temperature (24 h). After 24 h, the obtained MWC/ZIF, were separated by using a centrifuge, followed by repeatedly washing with methanol and dried for 24 h in a vacuum oven at 65ºC.

2.3. Batch sorption studies for removal of Pb(II) ions

In order to determine the amount of Pb(II) ion removal by the MWC/ZIF, adsorption tests were performed at ambient temperature and in a batch manner, and each study was repeated 3 times. For this assesses, the effective factors on the removal of Pb(II) ions such as concentration, temperature, pH of solution, time and ionic strength were investigated in an aqueous solution containing Pb(II) ion with a concentration of 80 mg L^{-1}. Adsorption experiments were further completed by adding 0.1 g MWC/ZIF into 50 mL of an aqueous solutions containing of Pb(II) ions in a 250-mL Erlenmeyer flask. The shaking of the mixtures was done using an IKA stirrer KS model at a speed of 300 rpm and for certain periods of time. After the adsorption of Pb(II) ion on the MWC/ZIF was completed, the mixtures were transferred to a centrifuge and then the concentration of Pb (II) ions in the supernatant solutions were measured using FAAS. The influence of the initial concentrations of Pb(II) ions (75 to 200 mg L^{-1}) on adsorption at the pH value of 5 was also examined. With respect to the obtained results, the concentration of 80 mg L^{-1} was used to investigate

DOI: 10.30473/ijac.2024.71788.1303

adsorption in further situations. The effect of the pH of the solution on removal of Pb(II) ions was correspondingly assessed from pH 2 to 5.5. Moreover, the adsorption thermodynamic was assessed at various temperatures (273, 280, 290, 298, and 310 K). Different concentrations of sodium chloride (0, 0.01, 0.05, 0.1, 0.25, and 0.5 M) were also utilized for assesses the impact of ionic strength on the Pb(II) ions removal. The removal percentage (Re%) was computed using Equation 1:

$$\text{Re}\ \% = \frac{C_0 - C_t}{C_0} \times 100 \qquad \text{Eq. (1)}$$

The amount of Pb(II) ion adsorbed by the MWC/ZIF after time t (q_t, mg g^{-1}) was also computed via Equation 2.

$$q_t = \frac{(C_0 - C_t)\,V}{W} \qquad \text{Eq. (2)}$$

Where, C_0 denoted to initial concentrations of Pb(II) ions (mg L^{-1}), C_t denoted to concentrations of Pb(II) ions (mg L^{-1}) after time *t*, *V* denoted to volume of solution (L) and *W* denoted to mass of MWC/ZIF (g)

2.4. Assesses of desorption

Desorption tests were fulfilled in a batch manner. As in adsorption tests, 0.1 g MWC/ZIF was added to 50 mL of an aqueous solution contain Pb(II) ions (80 mg L^{-1}) and stirred 30-min at 298 K. The MWC/ZIF adsorbents loaded with Pb(II) ions were then separated by a centrifuge.

Solvent desorption method was used for regeneration of the MWC/ZIF saturated with Pb(II) ions. For this study, 20 mL HCl was added to the MWC/ZIF saturated with Pb(II) and shake (300 rpm) for 30 min. Once desorption was completed, the adsorbent was separated from mixture, washed with deionized water, and in the following dried in an oven at 80 ºC for successive cycles. To check the reusability of the adsorbent used in the first step, the aforementioned adsorption-desorption experiment was repeated five times using the same adsorbent. The amount of Pb(II) ion absorbed per 1 gram of adsorbent in equilibrium conditions (q_e, mg/g) was calculated using equation 3:

$$q_e = \frac{(C_0 - C_t)\,V}{W} \qquad \text{Eq. (3)}$$

3. Results and Discussion

3.1. Characterization of MWC/ZIF nanocomposite

For investigation of functional groups onto surface of the carboxylic acid functionalized MWC and MWC/ZIF, the FT-IR spectra (Fig. 1) of these two materials was assessed (400 to 4000 cm^{-1}).

In Fig. 1a, the appeared band at 1633 cm^{-1} is due to the stretching vibration of C=C, which indicates that MWC have a graphitic structure. The appear band at 1721 cm^{-1} is due to the stretching vibration of C=O, which indicates the presence of carboxylic acid groups on the surface of carbon nanotubes. Also, the appear bands at 1022 and 3446 cm^{-1} are due to the C-O and O-H stretching vibrations of carboxylic acid groups, respectively. Symmetric and antisymmetric stretching vibrations of CH_2 were appeared at 2851 and 2920 cm^{-1}, respectively. In Fig. 1b, the appeared bands at 690 and 750 cm^{-1} were due to bending vibrations of 2-MeIm ring (out-of-plane). The appeared bands at 990-1310 cm^{-1} region were due to bending vibrations of the 2-MeIm ring (in-plane). The appeared bands at 1422 and 1455 cm^{-1} could be assigned to the stretching vibrations of the entire ring. The appeared bands that can be observed at 1582 and 1632 cm^{-1} could be assigned to the stretching vibrations of C=C and C=N in the 2-MeIm ring. The appeared bands that can be observed at 2925 and 3134 cm^{-1} could be assigned to the stretching vibrations of aliphatic and aromatic C-H bands in the 2-MeIm ring. The appeared band that can be observed at 420 cm^{-1} is due to the stretching vibration of Zn–N and Co–N [36]. A wide band that can be observed at 3446 cm^{-1} could be specified to the stretching vibrations of O-H groups.

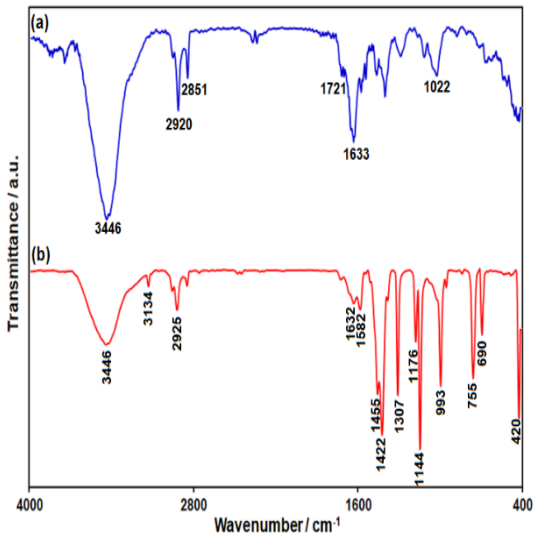

Fig. 1. FT-IR spectra of MWC (a) and MWC/ZIF nanocomposite (b).

The XRD spectrum (Fig. 2) was used for assesses of crystal structure of MWC/ZIF nanocomposite. High crystallinity and the phase purity of nanocomposite was confirmed by XRD pattern. The prominent and important peaks appearing in Fig. 2 are in good agreement with the X-ray peaks

DOI: 10.30473/ijac.2024.71788.1303

reported in previous papers [36,37]. In addition, the high intensity of nanocomposite peaks makes the peaks of carbon nanotubes not visible.

The field emission scanning electron microscopy (Fig. 3) (FE-SEM) was used for assesses of morphology and structure of the synthesized nanocomposite. The FE-SEM image showed that ZIF crystals with regular dodecahedron morphology are intertwined with carbon nanotubes.

The existence of Co, Zn, C, N, and O elements in the synthesized nanocomposite was confirmed by the EDS spectrum of nanocomposite (Fig. 4).

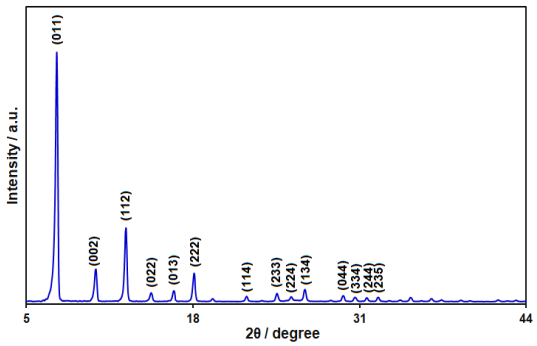

Fig. 2. XRD pattern of MWC/ZIF nanocomposite.

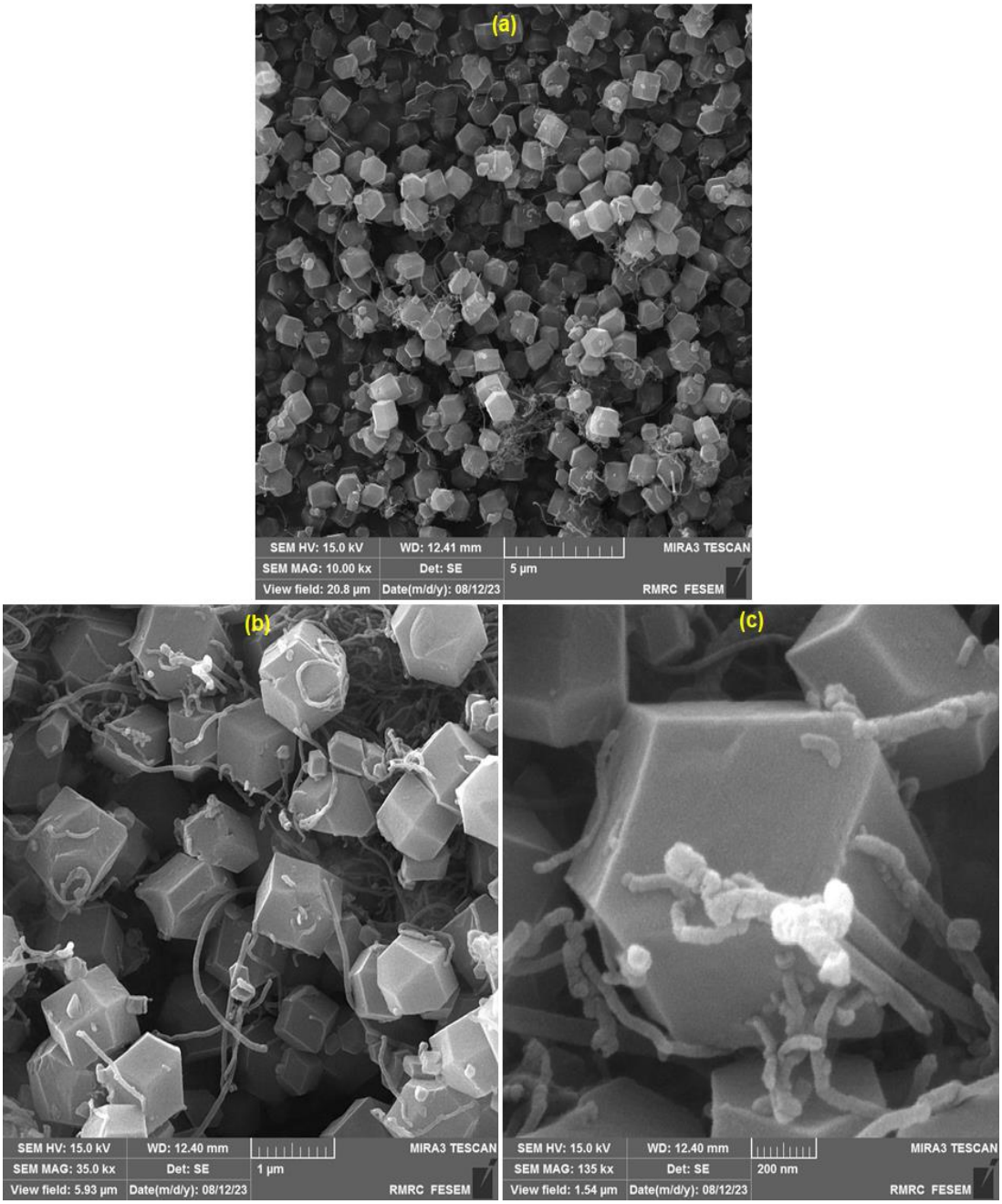

Fig. 3. FE-SEM images of MWC/ZIF nanocomposite with different magnifications: 10000 (a), 35000 (b), and 135000 (c)

DOI: 10.30473/ijac.2024.71788.1303

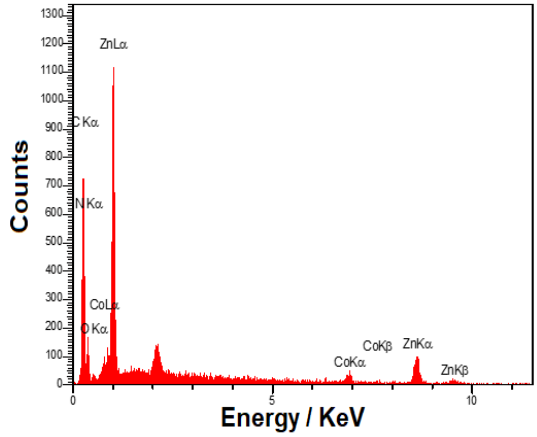

Fig. 4. EDS spectrum of MWC/ZIF nanocomposite.

3.2. The effect of pH

The pH of solution is a very important factor in the adsorption process because the functional groups on the surface of the adsorbent as well as the chemical structure of adsorbate could be affected by pH of solution [38,39]. Therefore, the effect of pH on the Re% of Pb(II) ion was evaluated over a pH range of 2-5.5 (Fig. 5a). The results showed that the maximum sorption of Pb(II) ions occurred in the pH range of 4.5-5.5. Since, at pHs higher than 5.5, Pb(II) ion could be precipitate in the form of $Pb(OH)_2$, therefore, pHs higher than 5.5 were not investigated in the present study. According to the results, other studies were carried out at pH 5.

3.3. The assesses of contact time and initial concentrations

The impact of initial concentration and contact time on the Re% of Pb(II) ion can be seen in the Fig. 6a and Fig. 5b, respectively.

According to Figure 5b, the Pb(II) adsorption enhances quickly in the early 20 min and reaches to balance at 30 min. With the start of the adsorption process, Pb(II) ions gradually occupy the active sites on the MWC/ZIF surface, in the next step, Pb(II) ions must be transferred from the bulk solution to the surface of the MWC/ZIF nanocomposite. This gradual diffusion would decline the sorption level of Pb(II) ions after 20 min.

Various initial concentrations of Pb(II) ions (75, 100, 125, 150 and 200 mg/L) were also used to examine the impact of initial concentration of Pb(II) ions on adsorption by the MWC/ZIF. According to Figure 6a, adsorption capacity of Pb(II) ions by the MWC/ZIF enhances when initial concentration of Pb(II) ions increases. By increasing the initial concentration of Pb(II) ions, the concentration gradient increases and acts as a driving force and as a result causes more absorption of Pb(II) ions [39]. Clearly, adsorption procedure largely depends on contact time and initial concentration of Pb(II) ions. Therefore, a contact time (30 minutes) and a C_0 (80 mg/L) can be chosen for other experiments.

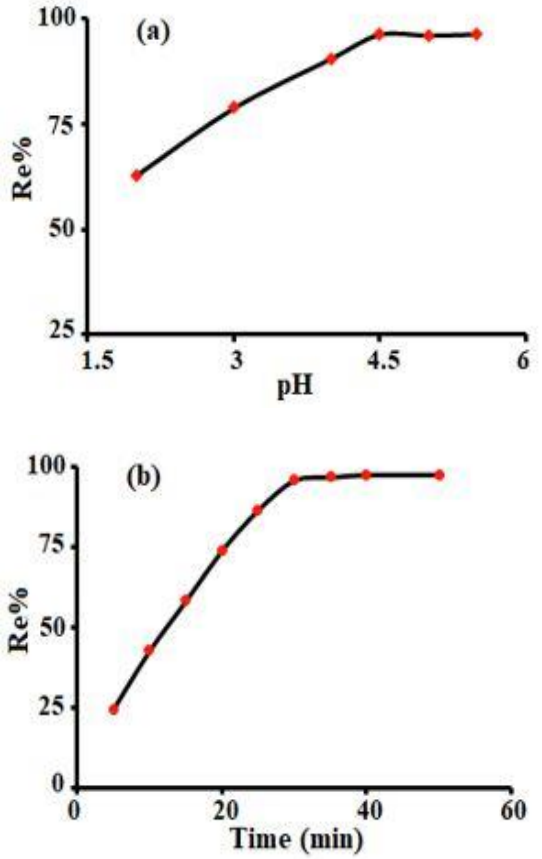

Fig. 5. (a) pH impact on Re% of Pb(II) ion. Conditions: 50 mL Pb(II) ion 80.0 mg L^{-1}. Agitation time: 30 minutes. Agitation velocity: 300 rpm. MWC/ZIF, 0.1 g and (b) The contact time effect on Re% of Pb(II) ion. Conditions were same as part (a) of this Figure except for the agitating time.

3.4 Adsorption isotherm

To explain the adsorption capacities of Pb(II) ions on the MWC/ZIF, the equilibrium experimental data was analyzed to assess the fitness of the data to the Langmuir, Freundlich, and Temkin isotherm models. The non-linear Langmuir isotherm model (Equation 4) is given in Eq. 4 [40]:

$$q_e = \frac{Q_0 K_L C_e}{(1+K_L C_e)} \quad (4)$$

In Eq. 4, the equilibrium concentration of Pb(II) ions (mg/L) has been denoted to Ce, the adsorbed Pb(II) ions (mg/g) in the equilibrium time has been denoted to q_e, the monolayer adsorption capacity of MWC/ZIF nanocomposite has been denoted to Q_0 (mg/g) and the Langmuir constant has been denoted to K_L(L/mg).

The Langmuir model assumes that adsorption occurs on a homogeneous surface with a finite number of identical sites, and the adsorption of one analyte does not affect the adsorption of another. Using the linear form of Langmuir isotherm model

DOI: 10.30473/ijac.2024.71788.1303

(Equation 5), we can obtain the Langmuir isotherm variables.

$$\frac{C_e}{q_e} = \frac{1}{Q_0 K_L} + \frac{C_e}{Q_0} \quad (5)$$

The plot of Ce/qe versus Ce is a straight line with a slope of $1/Q_0$ and an intercept of $1/Q_0K_L$. The values of Q_0 and K_L can be obtained from the slope and intercept of the linear plot, respectively (as shown in Fig. 6b).

According to Table 1, the Langmuir isotherm parameters Q_0 and K_L were determined to be 81.3 mg/g and 0.193 L/mg, respectively, with a correlation coefficient (R) value of 0.9986. The highest monolayer adsorption capacity for Pb(II) ions onto the MWC/ZIF at 298 K was found to be 81.3 mg/g. This suggests that the MWC/ZIF has a good adsorption capacity for removal of Pb(II) ions from aqueous solutions.

Table 1. The isotherm constants to adsorb Pb(II) ions onto the surface of MWC/ZIF.

Isotherm models	constants	Value
Langmuir	Q (mg/g)	81.3
	K_L (L/g)	0.193
	R^2	0.9973
Freundlich	K_f (mg/g)	27.68
	1/n	0.261
	R^2	0.9866
Temkin	K_t (L/mol)	4.32
	B	13.839
	R^2	0.9928

The Freundlich isotherm is another empirical equation used to describe adsorption on a heterogeneous surface. It assumes that the adsorption occurs at sites with different adsorption energies, and the amount of adsorbate adsorbed increases with increasing of concentration. The linearized form of the Freundlich isotherm equation is given by Equation 6 [41]:

$$\log q_e = \log K_f + \frac{1}{n} \log C_e \quad (6)$$

where q_e is the amount of adsorbed Pb(II) at equilibrium (mg/g), Ce is the equilibrium concentration of Pb(II) ions (mg/L), K_f is the Freundlich constant related to the adsorption capacity $(mg/g)*(L/mg)^{(1/n)}$, and n is the Freundlich exponent related to the intensity of adsorption.

The plot of log (q_e) versus log (C_e) is a straight line with a slope of 1/n and an intercept of log(K_f). The values of n and K_f can be obtained from the slope and intercept of the linear plot, respectively (as shown in Figure 6c).

Table 1 presents the Freundlich isotherm parameters for the adsorption of Pb(II) ions onto surface of MWC/ZIF. The value of n, which is an experimental parameter, changes with the degree of inhomogeneity of the bonded Pb(II) ions on the surface of adsorbent. The n value greater than 1 indicates the optimal adsorption. The value of K_f indicates the capacity of Pb(II) ions adsorption. In addition, the higher the value of n, the more significant the absorption intensity [41].

The linear form of the Temkin isotherm is expressed by Equation 7 [41]:

$$q_e = B \ln K_t + B \ln C_e \quad (7)$$

The adsorbate-adsorbent interactions considered by Temkin isotherm and assumes that the heat of adsorption decreases linearly with the covering the absorbent surface by the adsorbate substance. In Eq. 7, q_e and C_e have the same definitions as before, *B* refers to the Temkin constant associated with the adsorption heat, and K_t refers to the constant of equilibrium (L/mg).

The plot of q_e versus ln (C_e) is a straight line with slope of *B* and an intercept of *B* ln (K_t). *B* and K_t can be obtained from the slope and intercept of the resulting line, respectively. The linear plot of q_e versus ln (C_e) for the adsorption of Pb(II) ions on the MWC/ZIF was showed in Figure 6d.

Table 1 provides the Temkin constants and R^2 value for the adsorption of Pb(II) ions on the MWC/ZIF. These constants give information about the adsorption heat and maximum binding energy of the adsorbate on the adsorbent.

Table 1 indicates that the Langmuir model provides a better fit to the experimental data, as evidenced by its higher R^2 value. The maximum monolayer adsorption capacity for Pb(II) ions on the MWC/ZIF was found to be 81.3 mg/g at 25°C. Since the value of n in the Freundlich equation (3.831) is between 1 and 10, therefore the absorption of Pb(II) ions is favorable [41].

Table 2 presents a comparison of the highest monolayer adsorption capacity of Pb(II) ion on various adsorbents in previous studies [1,17-24, 42-46]. The adsorption capacity of MWC/ZIF obtained in this study was found to be comparable to or greater than the reported amounts in several previous studies [19, 23, 42-46]. Additionally, the removal of Pb(II) ion by MWC/ZIF was faster compared to most of the previous studies [1, 17, 20,22,24, 42-46], indicating that MWC/ZIF could be an excellent adsorbent for removing Pb(II) ion from wastewater samples.

3.5. Kinetic examination

To assesses of Pb(II) adsorption kinetics on the MWC/ZIF, the intraparticle diffusion model (IPD), the Lagergren's pseudo-first and second-order models and the Elovich model were assessed. The pseudo-first order model (Equation 8) is as follows [46]:

$$\ln (q_e - q_t) = \ln q_e - K_1 t \quad (8)$$

In Equation 8, q_t and q_e represent the amount of Pb(II) ions adsorbed (mg/g) at any time t (min) and at equilibrium, respectively. K_1 is the rate constant

DOI: 10.30473/ijac.2024.71788.1303

of the pseudo-first order sorption (min^{-1}). The value of q_e and K_1 can be determined from the intercept and the slope of the plot of $\log(q_e-q_t)$ versus t, as shown in Figure 7a.

Pseudo second-order model is defined as follows (Eq. 9) [46]:

$$\frac{dq_t}{dt} = k_2(q_e - q_t)^2 \quad (9)$$

Rearranging the variables gives (Eq. 10):

$$\frac{dq_t}{(q_e-q_t)^2} = k_2 dt \quad (10)$$

When equation 10 has been integrated in the boundary conditions t=0 (q=0) to t=t (q=qt), equation 11 has been obtained.

$$\frac{t}{q_t} = \frac{1}{K_2 q_e^2} + \frac{t}{q_e} \quad (11)$$

In the above equation, K_2 represents the rate constant of pseudo-second order adsorption (g/mg min). The value of q_e and K_2 can be also calculated from slope and intercept of plot (t/qt versus t), as shown in Figure 7b.

The Elovich equation was also used to qualitatively describe the chemisorption process [41]. The linear form of the Elovich model is expressed by Equation 12:

$$q_t = \frac{1}{\beta} ln\, \alpha\beta + \frac{1}{\beta} ln\, t \quad (12)$$

In Equation 12, α (g/mg min) refers to the sorption rate and β (g/mg) refers to activation energy of chemisorption. The sorption rate (α) represents the rate at which the adsorbate molecules are chemically bonded to the surface of the adsorbent. The activation energy (β) represents the minimum energy required for the adsorbate molecules to overcome the energy barrier and form chemical bonds with the adsorbent surface. The values of α and β can be determined from the plot of q_t versus ln t, as shown in Figure 7c.

In the intraparticle diffusion model, the plot of q_t versus $t^{1/2}$ gives a straight line, which can be expressed by Equation 13 [47]:

$$q_t = K_{id}\, t^{\frac{1}{2}} + C \quad (13)$$

In this equation, the rate constant of intraparticle diffusion (mg/g $min^{1/2}$) was denoted to K_{id} and the intercept of the line denoted to C (Figure 7d).

The resulted kinetic parameters from these models summarizes in Table 3. The calculated q_e value for the Elovich model is in close agreement with the experimental q_e value, indicating a good fit of this model to the experimental data. The K_{id} for Pb(II) was 7.633 mg/g $min^{1/2}$, which shows the high tendency of the MWC/ZIF for removal of Pb(II) ions [48].

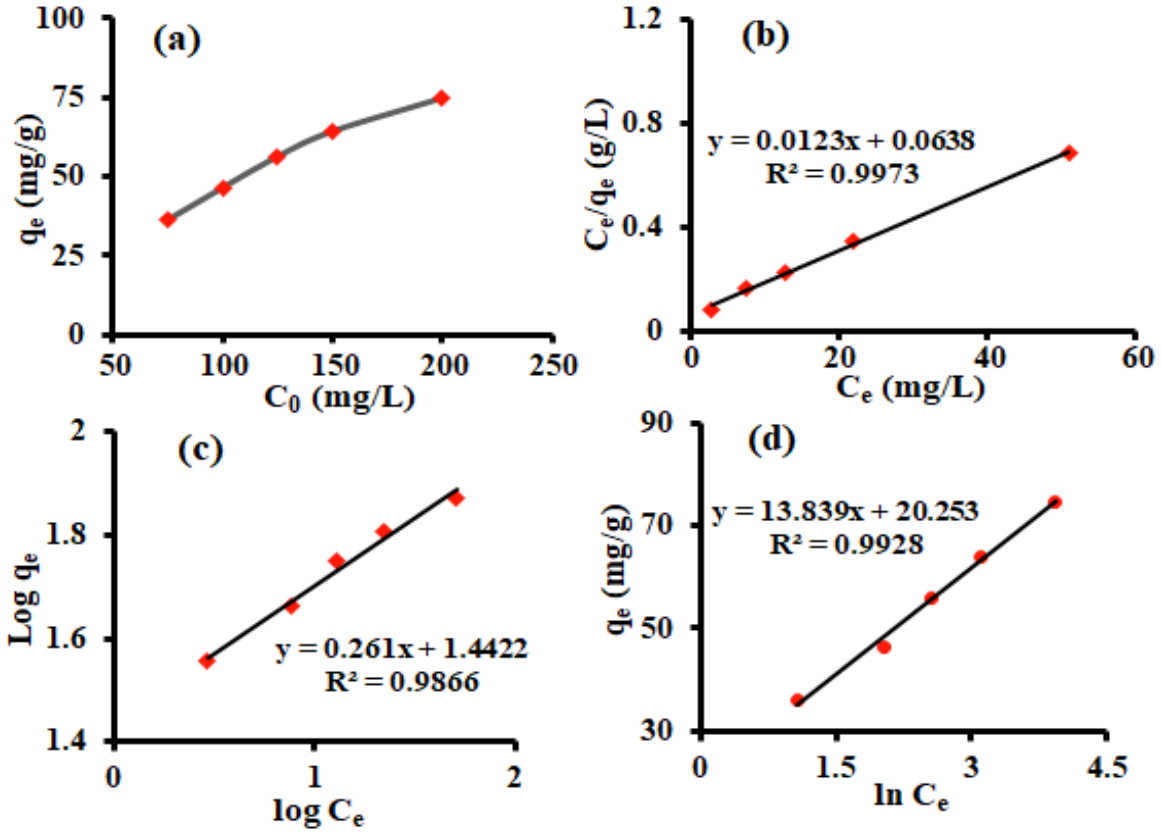

Fig. 6. (a) The impact of initial concentrations of Pb(II) ions, (b) Langmuir, (c) Freundlich and (d) Temkin adsorption isotherms to adsorb Pb(II) ions onto the MWC/ZIF at room temperatures.

DOI: 10.30473/ijac.2024.71788.1303

Table 2. Comparing the adsorption power of MWC/ZIF with the additional prepared adsorbents.

Adsorbent	Equilibrium time (min)	Q^0 (mg g^{-1})	Ref.
Chitosan cross-linked and grafted with epichlorohydrin and 2,4-dichlorobenzaldehy	60	170	[1]
chemical modification of activated carbon by 2-aminothiazole	60	310.9	[17]
Activated carbon	20	200	[18]
Activated carbon	25	90.91	[19]
Polyacrylic acid capped Fe_3O_4 – Cu-MOF hybrid	60	641	[20]
Ninhydrin-functionalized chitosan	120	196	[21]
Melon Peel as a bioadsorbent	40	191.9	[22]
Modified Cassia fistula seeds-	30	13.2-129.3	[23]
Co3O4@SiO2 magnetic nanoparticle-nylon 6	70	666.7	[24]
Modified chitosan	120	55.55	[42]
Epichlorohydrin crosslinked chitosan Schiff's base@Fe3O4	105	86.2	[43]
Chitosan derivatives beads	100	34.98	[44]
Chitosan-vanillin derivatives	240	66.23	[45]
magnetic activated carbon–cobalt nanoparticles	30	312.5	[46]
MWC/ZIF	30	81.3	This work

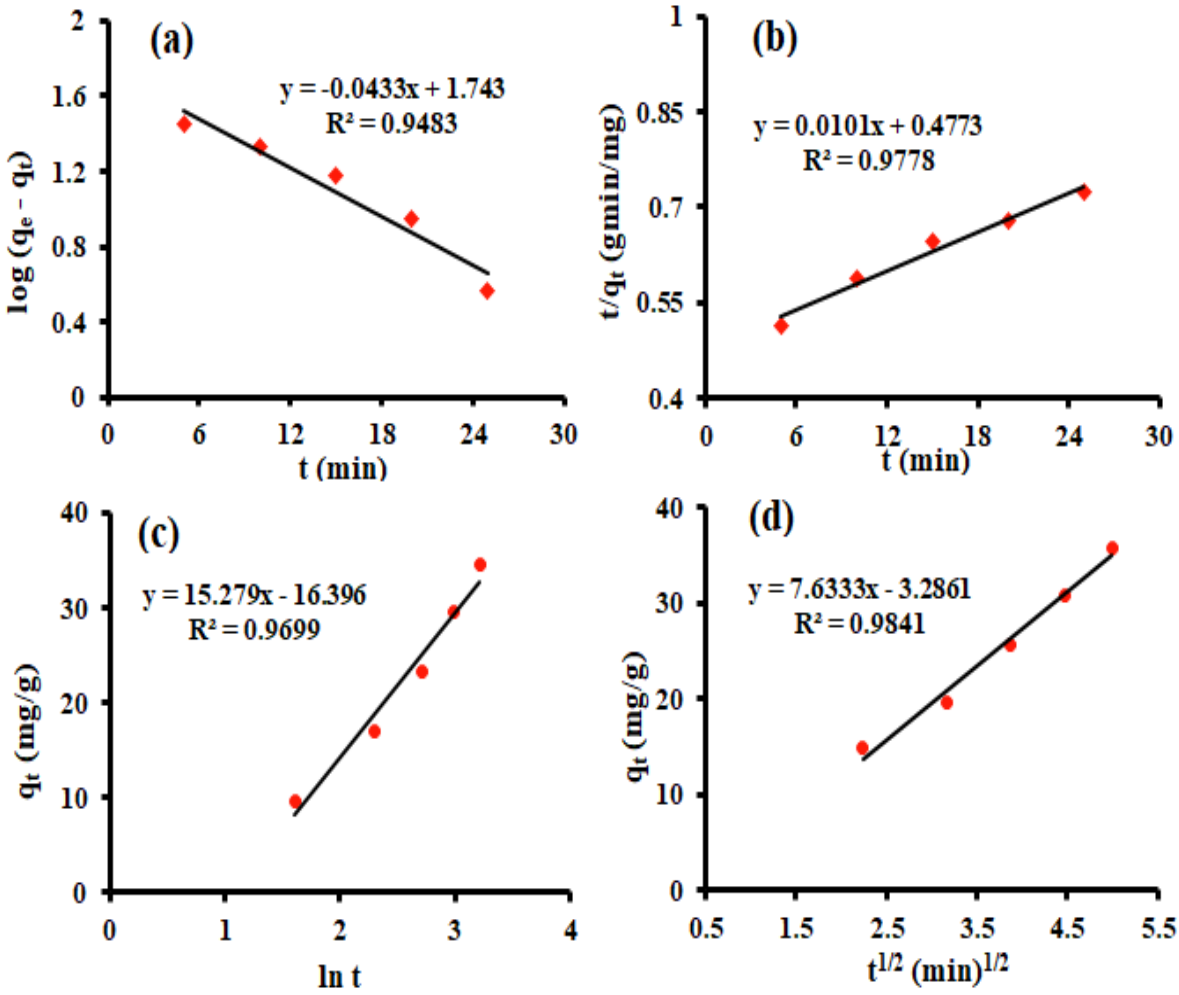

Fig. 7. The Pb(II) ions adsorption kinetic onto the MWC/ZIF at room temperature: (a) pseudo first order, (b) pseudo second order, (c) Elovich and (d) intraparticle diffusions plots.

DOI: 10.30473/ijac.2024.71788.1303

Table 3. Kinetics constants for Pb(II) sorption onto the MWC/ZIF.

Kinetics model	Coefficients	Value
	q_e experimental (mg/g)	38.28
Pseudo first order	k_1 (1/min)	0.0433
	q_e calculated (mg/g)	5.71
	R^2	0.9483
Pseudo second order	k_2 (g/mg min)	2.137
	q_e calculated (mg/g)	99.01
	R^2	0.9778
Elovich model	α (mg/ g min)	5.26
	β (g/mg)	0.0654
	q_e calculated (mg/g)	35.57
	R^2	0.9699
Intra-particle diffusion model	k_{id} (mg/g $min^{1/2}$)	7.633
	q_e calculated (mg/g)	38.5
	R^2	0.9841

3.6. Thermodynamic analysis

In order to define the related mechanisms, thermodynamic examinations were done at different temperatures. Equations 14 and 15 were also used to estimate various thermodynamic variables, including changes in standard free energy (ΔG°), enthalpy (ΔH°), and entropy (ΔS°) [49]:

$$Log\ K_C = \frac{\Delta S^0}{2.303\ R} - \frac{\Delta H^0}{2.303\ RT} \quad (14)$$

$$\Delta G^0 = \Delta H^0 - T\Delta S^0 \quad (15)$$

where R(J·mol^{-1}·K^{-1}) refers to the gas constant, T(K) refers to the absolute temperature and Kc refers to the thermodynamic equilibrium constant. The values of ΔS° and ΔH° were calculated from the intercept and slope of the plot of log Kc versus 1/T, as shown in Figure 8. Table 4 summarizes the different thermodynamic variables at five temperatures. The results indicate that the values of ΔG° were negative at each temperature, suggesting the spontaneity of the adsorption process of Pb(II) ion on the active adsorption sites. The decrease in ΔG° values with increasing temperature indicates that the higher temperatures facilitate the adsorption of Pb(II) ion on the MWC/ZIF.

Moreover, changes in the ΔH° enthalpy (43.35 kj/mol) were positive, implying endothermic feature due to enhancement of adsorption on later enhancements in temperatures. However, positive values of ΔS°(172.35 j/mol) showed the higher randomness at the solid liquid solution interface.

Table 4. Thermo-dynamic variables to adsorb Pb(II) on the MWC/ZIF.

T (K)	275	282	288	298	309
ΔG^0 (j/mol)	- 4271.4	- 5184.2	- 5930.6	- 8127.4	- 9998.2
ΔH^0 (kj/mol)		43.35			
ΔS^0 (j/mol)		172.35			

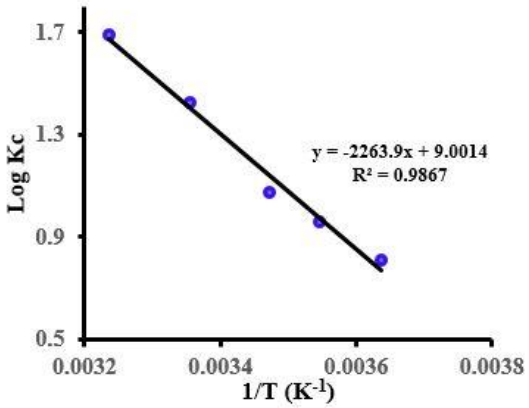

Fig. 8. Thermo-dynamic examination of Pb(II) ions adsorption on MWC/ZIF

3.7. Impact of ionic strength

It is known that wastewater mostly contains common ions; therefore, the impact of ionic strength on Pb(II) adsorption was studied by addition of NaCl (0, 0.01, 0.05, 0.1, 0.25, and 0.5 M) to a solution containing 80 ppm Pb(II) ion at pH=5. The results in Figure 9 showed that with increasing of NaCl concentration, the removal efficiency of lead (II) ions decreases slightly. The reason for this phenomenon may be the competitive adsorption of NaCl and Pb(II) ion to occupy places on the absorbent surface [46].

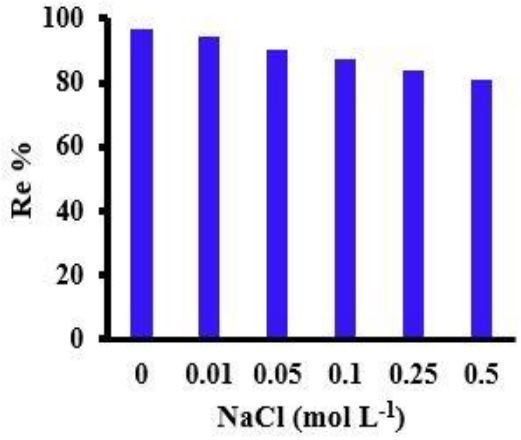

Fig. 9. Ionic strength impact on adsorption of Pb(II) ions onto the MWC/ZIF.

3.8. MWC/ZIF reusability

Adsorbent reusability is a leading factor in the environmentally-friendly and economical process of adsorption. The problem with contaminated

adsorbent disposal to the environment may be thus decreased due to adsorbent reusability. The results (Fig. 10) demonstrated that the Re% of Pb(II) ion dropped to 80.9% at the fifth round from 97.8% at the first cycle, that indicating the excellent reusability performance of MWC/ZIF in removing Pb(II) ion.

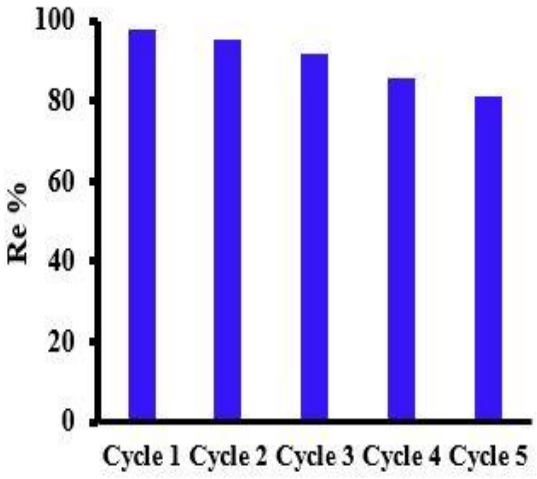

Fig. 10. Reusability test to adsorb Pb(II) ions onto the MWC/ZIF at room temperatures. Condition has been similar to Figure 5 using the same adsorbent.

3.9. Treatment of wastewater sample

The real wastewater samples were collected from an industrial center in Kerman Province, Iran, and then examined for the respective content using inductively coupled plasma-optical emission spectrometry (ICP-OES) as shown in Table 5. In the next step, real wastewater sample was spiked with Pb(II) ion (80 mg/L) and treated with the MWC/ZIF under optimized conditions. The mixture was then separated and analyzed for metal ion levels using ICP-OES (Table 5). The results showed that the MWC/ZIF was highly efficient in removing Pb(II) ions and some metal ions from the wastewater samples.

Table 5. Application of the MWC/ZIF to remove Pb(II) ions from wastewater sample.

Metal ions	Concentration before treatment (mg/L)*	Concentration after treatment (mg/L)	Re (%)
Pb	83.8	4.1	95.1
Cr	3.9	0.3	92.3
As	4.1	0.2	95.1
Cu	6.5	0.4	93.8
Ni	4.4	0.6	86.4
Cd	5.3	0.3	94.3
Mn	3.8	0.2	94.7
Co	4.7	0.5	89.4

*Original sample spiked with 80 mg/L of Pb(II) ion.

4.CONCLUSION

In this study, multiwall carbon nanotube/ZnCo-Zeolite imidazole framework was developed as an effective adsorbent for removal of Pb(II) ions from wastewater samples. The successful synthesis of MCN/ZIF confirmed by the obtained results from FT-IR, SEM, XRD and XPS analyses. The applicability of the MCN/ZIF as an efficient adsorbent was further confirmed by its ability to effective removal of Pb(II) ions from an effluent sample. The equilibrium data showed that the adsorption of Pb(II) ion follows the Langmuir isotherm model and the highest adsorption capacity of Pb(II) ion on the MCN/ZIF surface using this model was 81.3 mg/g. The desorption experiment results showed that the MCN/ZIF can be recovered and reused for up to five cycles. The assesses of the adsorption kinetics showed that the adsorption of Pb(II) ion on the adsorbent follows the Elovich equation. The results of the thermodynamic study showed that the adsorption of Pb(II) ion on the adsorbent surface is spontaneous and is an endothermic process.

ACKNOWLEDGEMENTS

The authors wish to thank Payame Noor University for support of this work.

REFERENCES

[1]L. Xiao, H. Shan, and Y. Wu, Chitosan cross-linked and grafted with epichlorohydrin and 2,4-dichlorobenzaldehyde as an efficient adsorbent for removal of Pb(II) ions from aqueous solution, *Int. J. Biol. Macromol.* 247 (2023) 125503.

[2]M. Kaur, P. Sharma, and S. Kumari, Response surface methodology approach for optimization of Cu2+ and Pb2+ removal using nanoadsorbent developed from rice husk, *Mater. Today Commun.* 21 (2019) 1–10.

[3]S. Haider, F.A.A. Ali, A. Haider, W.A. Al-Masry, and Y. Al-Zeghayer, Novel route for amine grafting to chitosan electrospun nanofibers membrane for the removal of copper and lead ions from aqueous medium, *Carbohydr. Polym.* 199 (2018) 406–414.

[4]Y. Zhang, M. Zhao, Q. Cheng, C. Wang, H. Li, X. Han, Z. Fan, G. Su, D. Pan, and Z. Li, Research progress of adsorption and removal of heavy metals by chitosan and its derivatives, *a review, Chemosphere* 279 (2021) 130927.

[5] S. Begum, N.Y. Yuhana, N. Md Saleh, and N.H. Nazirah Kamarudin, A.B. Sulong, Review of chitosan composite as a heavy metal adsorbent: material preparation and properties, *Carbohydr. Polym*. 259 (2021) 117613.

[6] P. Abhari, S. Abdi, and M. Nasiri, Effect of various types of anions and anionic surfactants on

the performance of micellar enhanced ultrafiltration process in the removal of Pb(II) ions: An optimization with the response surface methodology, *Chem. Eng. Res. Des.* 187 (2022) 332–346.

[7] D, D, Giri, A. Alhazmi, A. Mohammad, S. Haque, N. Srivastava, V.K. Thakur, V.K. Gupta, and D.B. Pal, Lead removal from synthetic wastewater by biosorbents prepared from seeds of Artocarpus heterophyllus and Syzygium cumini, *Chemosphere* 287 (2020) 132016.

[8] A. Dabrowski, Z. Hubicki, P. Podkos´cielny, and E. Robens, Selective removal of the heavy metal ions from waters and industrial wastewaters by ion-exchange method, *Chemosphere* 56 (2004) 91–106.

[9] A. Bodagh, H. Khoshdast, H. Sharafi, H. Shahbani Zahiri, and K. Akbari Noghabi, Removal of cadmium (II) from aqueous solution by ion flotation using rhamnolipid biosurfactant as an ion collector, *Ind. Eng. Chem. Res*. 52 (2013) 3910–3917.

[10]G.Z. Kyzas, E.A. Deliyanni, K.A. Matis, Graphene oxide and its application as an adsorbent for wastewater treatment, *J. Chem. Technol. Biotechnol*. 89 (2014) 196–205.

[11]M.M. Matlock, B.S. Howerton, D.A. Atwood, Chemical precipitation of lead from lead battery recycling plant wastewater, *Ind. Eng. Chem. Res.* 41 (2002) 1579–1582.

[12]O. Agboola, T. Mokrani, R. Sadiku, Porous and fractal analysis on the permeability of nanofiltration membranes for the removal of metal ions, *J. Mater. Sci*. 51 (2016) 2499–2511.

[13]F.M. Pang, P. Kumar, T.T. Teng, A.K. Mohd Omar, K.L. Wasewar, Removal of lead, zinc and iron by coagulation-flocculation, *J. Taiwan Inst. Chem. Eng. 42* (2011) 809–815.

[14]Y.X. Liu, J.M. Yan, D.X. Yuan, Q.L. Li, X.Y. Wu, The study of lead removal from aqueous solution using an electrochemical method with a stainless steel net electrode coated with single wall carbon nanotubes, *Chem. Eng. J*. 218 (2013) 81–88.

[15]Y. Jia, Y. Zou, X. Zou, Y. Jiang, S. Song, J. Qin, Y. Wang, L. Zhu, Study on the adsorption performance of multi-base composite magnesia cementitious material microfiltration membrane for different heavy metal ions, *Mater. Lett.* 335 (2023) 133488.

[16] X. Zeng, G. Zhang, J. Zhu, and Z. Wu, Adsorption of heavy metal ions in water by surface functionalized magnetic composites: *a review*, *Environ. Sci. Water Res. Technol*. 8 (2022) 907–925.

[17]S.M. Waly, A.M. El-Wakil, and W.M. Abou El-Maaty, F.S. Awad, Efficient removal of Pb(II) and Hg(II) ions from aqueous solution by amine and thiol modified activated carbon, *J. Saudi Chem. Soc*. 25 (2021) 101296.

[18]S. Z. Mohammadi, H. Hamidian, and Z. Moeinadini, High surface area-activated carbon from Glycyrrhiza glabra residue by ZnCl2 activation for removal of Pb(II) and Ni(II) from water samples, *J. Ind. Eng. Chem.* 20 (2014) 4112–4118.

[19]S. Z. Mohammadi, M.A. Karimi, S.N. Yazdy, T. Shamspur, and H. Hamidian, Removal of Pb(II) ions and malachite green dye from wastewater by activated carbon produced from lemon peel, *Quim. Nova* 37 (2014) 804-809.

[20]P. Goyal, C. Shekhar Tiwary, and S. K. Misra, Ion exchange based approach for rapid and selective Pb(II) removal using iron oxide decorated metal organic framework hybrid, *J. Environ. Manag.* 277 (2021) 111469.

[21]Y. Chen, J. Tang, S. Wang, L. Zhang, Ninhydrin-functionalized chitosan for selective removal of Pb(II) ions: Characterization and adsorption performance, *Int. J. Biol. Macromol*. 177 (2021) 29–39.

[22]H. Ahmadi, S.S. Hafiz, H. Sharifi, N. Ngambua Rene, S. Sanaullah Habibi, and S. Hussain, Low cost biosorbent (Melon Peel) for effective removal of Cu (II), Cd (II), and Pb (II) ions from aqueous solution, *Case Stud. Chem. Environ. Eng.* 6 (2022) 100242.

[23]R.V. Hemavathy, A. Saravanan, P. Senthil Kumar, D.-V.N. Vo, S. Karishma, and S. Jeevanantham, Adsorptive removal of Pb(II) ions onto surface modified adsorbents derived from Cassia fistula seeds: Optimization and modelling study, *Chemosphere* 283 (2021) 131276.

[24]S.Z. Mohammadi, Z. Safari, and N. Madady, A novel Co3O4@SiO2 magnetic nanoparticle-nylon 6 for high efficient elimination of Pb(II) ions from wastewater, *Appl. Surf. Sci*. 514 (2020) 145873.

[25]Z. Jafari, V.M. Avargani, and M.R. Rahimi, Magnetic nanoparticles-embedded nitrogen-doped carbon nanotube/porous carbon hybrid derived from a metal-organic framework as a highly efficient adsorbent for selective removal of Pb(II) ions from aqueous solution, *J. Mol. Liq*. 318 (2020) 113987.

[26]R. Sitko, M. Musielak, M. Serda, E. Talik, A. Gagor, B. Zawisza, and M. Malecka, Graphene oxide decorated with fullerenol nanoparticles for

highly efficient removal of Pb(II) ions and ultrasensitive detection by total-reflection X-ray fluorescence spectrometry, *Sep. Pur. Technol*. 277 (2021) 119450.

[27]M.D. Yahya, I.B. Muhammed, K.S. Obayomi, A.G. Olugbenga, and U.B. Abdullahi, Optimization of fixed bed column process for removal of Fe(II) and Pb(II) ions from thermal power plant effluent using NaoH-rice husk ash and Spirogyra, *Sci. Afr*. 10 (2020) e00649.

[28]R. Kasirajan, A. Bekele, E. Girma, Adsorption of lead (Pb-II) using CaO-NPs synthesized by sol gel process from hen eggshell: Response surface methodology for modeling, optimization and kinetic studies, *S. Afr. J. Chem. Eng.* 40 (2022) 209–229.

[29]J. Bayuoa, M. Rwiza, M. Abdullai Abukari, K.B. Pelig-Ba, and K. Mtei, Modeling and optimization of independent factors influencing lead(II) biosorption from aqueous systems: A statistical approach, *Sci. Afr*. 16 (2022) e01270.

[30]S.Z. Mohammadi, N. Mofidinasab, and M.A. Karimi, F. Mosazadeh, Fast and efficient removal of Pb(II) ion and malachite green dye from wastewater by using magnetic activated carbon–cobalt nanoparticles, *Water Sci. Technol.* 82 (2020) 829-842.

[31]M. Konni, S. Doddi, A.S. Dadhich, and S. Babu Mukkamala, Adsorption of CO2 by hierarchical structures of f-MWCNTs@Zn/Co-ZIF and N-MWCNTs@Zn/Co-ZIF prepared through in situ growth of ZIFs in CNTs, *Surf. Interfaces* 12 (2018) 20-25.

[32]K. Chhetri, A. Adhikari, J. Kunwar, D. Acharya, R. Mangal Bhattarai, Y.S. Mok, A. Adhikari, A. Prasad Yadav, and H. Yong Kim, Recent Research Trends on Zeolitic Imidazolate Framework-8 and Zeolitic Imidazolate Framework-67-Based Hybrid Nanocomposites for Supercapacitor Application, *Int. J. Energy Res.* 2023 (2023) 8885207.

[33]M. Shahsavari, I. Sheikhshoaie, and H. Beitollahi, Electrochemical sensor based on Fe3O4/ZIF-4 nanoparticles for determination of bisphenol A, *J. Food Meas. Charact.* 17 (2023) 1109-1118.

[34]R. Ahmad, U. Ali Khan, N. Iqbal, and T. Noorb, Zeolitic imidazolate framework (ZIF)-derived porous carbon materials for supercapacitors: an overview, *RSC Adv.* 10 (2020) 43733.

[35]C. Zhang, J. Ren, Y. Xing, M. Cui, N. Li, P. Liu, X. Wen, and M. Li, Fabrication of hollow ZnO-Co3O4 nanocomposite derived from bimetallicorganic frameworks capped with Pd nanoparticles and MWCNTs for highly sensitive detection of tanshinol drug, *Mater. Sci. Eng. C* 108 (2020) 110214.

[36]Q. Luo, X. Huang, Q. Deng, X. Zhao, H. Liao, H. Deng, and J. Jiang, Novel 3D cross-shaped Zn/Co bimetallic zeolite imidazolate frameworks for simultaneous removal Cr (VI) and Congo Red. Environ, *Sci. Poll. Res.* 29 (2022) 40041-40052.

[37]K. Zhou, B. Mousavi, Z. Luo, S. Phatanasri, S. Chaemchuen, and F. Verpoort, Characterization and properties of Zn/Co zeolitic imidazolate frameworks vs. ZIF-8 and ZIF-67, *J. Mater. Chem. A.* 5 (2017) 952-957.

[38]R. Istratie, R. Băbuță, A. Popa, C. Păcurariu, and M. Stoia, Enhanced Adsorption of p-Nitrophenol from Aqueous Solutions Using a Functionalized Styrene-Divinylbenzene Copolymer, *Water Air Soil Pollut.* 228 (2017) 276.

[39]W.O. Afolabi, B.O. Opeolu, O.S. Fatoki, B.J. Ximba, and O.S. Olatunji, Vitis vinifera leaf litter for biosorptive removal of nitrophenols, *Int. J. Environ. Sci. Technol.* 15 (2018) 1669–1678.

[40] P.-T. Huong, B.-K. Lee, J. Kim, and C.-H. Lee, Nitrophenols removal from aqueous medium using Fe-nano mesoporous zeolite, *Mater. Design* 101 (2016) 210–217.

[41]J. Chen, X. Sun, L. Lin, X. Dong, and Y. He, Adsorption removal of o-nitrophenol and p-nitrophenol from wastewater by metal organic framework Cr-BDC, *Chin. J. Chem. Eng.* 225 (2017) 775–781.

[42]G. Yuvaraja, Y. Pang, D.Y. Chen, L.J. Kong, S. Mehmood, M.V. Subbaiah, D.S. Rao, C.M. Pavuluri, J.C. Wen, and G.M. Reddy, Modification of chitosan macromolecule and its mechanism for the removal of Pb(II) ions from aqueous environment, *Int. J. Biol. Macromol.* 136 (2019) 177–188.

[43]Y. Yan, G. Yuvaraja, C. Liu, L. Kong, K. Guo, G.M. Reddy, and G.V. Zyeyanov, Removal of Pb(II) ion from aqueous media using epichlorohydrin crosslinked chitosan Schiff's base@Fe3O4 (ECCSB@Fe3O4), *Int. J. Biol. Macromol.* 117 (2018) 1305–1313.

[44]W.S.W. Ngah, and S. Fatinathan, Pb(II) biosorption using chitosan and chitosan derivatives beads: equilibrium, ion exchange and mechanism studies, *J. Environ. Sci.* 22 (2010) 338–346.

[45] F. Alakhras, H. Al-Shahrani, E. Al-Abbad, F. Al-Rimawi, and N. Ouerfelli, Removal of Pb (II) metal ions from aqueous solution using chitosan-vanillin derivatives of chelating polymers, *Pol. J. Environ. Stud.* 28 (2019) 1523–1534.

[46]S.Z. Mohammadi, N. Mofidinasab, M.A. Karimi, and F. Mosazadeh, Fast and efficient removal of Pb(II) ion and malachite green dye from wastewater by using magnetic activated carbon–

cobalt nanoparticles, *Water Sci. Technol.* 82 (2020) 829–842.

[47]A. dos Santos, M.F. Viante, D.J. Pochapski, A.J. Downs, and C.A.P. Almeida, Enhanced removal of p-nitrophenol from aqueous media by montmorillonite clay modified with a cationic surfactant, *J. Hazard. Mater.* 355 (2018) 136–144.

[48]Y. Tan, Z. Sun, H. Meng, Y. Han, J. Wu, J. Xu, Y. Xu, and X. Zhang, A new MOFs/polymer hybrid membrane: MIL-68(Al)/PVDF, fabrication and application in high-efficient removal of p-nitrophenol and methylene blue, *Sep. Pur. Technol.* 215 (2019) 217–226.

[49]R.K. Gautam, P.K. Gautam, S. Banerjee, S. Soni, S.K. Singh, and M.C. Chattopadhyaya, Removal of Ni(II) by magnetic nanoparticles, *J. Mol. Liq.* 204 (2015) 60-69.

DOI: 10.30473/ijac.2024.71788.1303

حذف جذبی یون‌های سرب (II) با استفاده از نانولوله‌های کربنی چند دیواره/ چارچوب‌های ایمیدازول زئولیتی روی کبالت: مطالعه بهینه‌سازی و مدل‌سازی

سید ضیاء محمدی[۱]، ساره ترابیان[۱،*]، سمیه تاجیک[۲،*]

۱- بخش شیمی، دانشگاه پیام نور، تهران، ایران
۲- مرکز تحقیقات بیماریهای گرمسیری و عفونی، دانشگاه علوم پزشکی کرمان، ایران، کرمان
* E-mail: Email: szmohammadi@pnu.ac.ir

تاریخ دریافت: ۲۴ تیر ۱۴۰۳ **تاریخ پذیرش:** ۱۸ مرداد ماه ۱۴۰۳

چکیده

یک جاذب کارآمد تحت عنوان نانولوله کربنی چند دیواره/چهارچوب ایمیدازول زئولیتی-روی کبالت(MWC/ZIF) تهیه شد و برای خارج کردن یون سرب از نمونه‌های پساب مورد استفاده قرار گرفت. بعد از جدا کردن جاذب از محلول، مقدار یون سرب موجود در محلول بوسیله دستگاه جذب اتمی مورد اندازه گیری قرار گرفت. بر این اساس، انواع پارامترهای تجربی موثر بر روی حذف یون سرب همچون pH، قدرت یونی، زمان، دما و غلظت یون سرب مورد بررسی قرار گرفت. برای بررسی سینتیک جذب یون سرب بر روی نانوکامپوزیت MWC/ZIF، انواع مدلهای سینتیکی مورد بررسی قرار گرفت. با توجه به یافته‌ها، نانوکامپوزیت تولید شده به عنوان یک روش جذبی موثر برای حذف یون سرب از نمونه های پساب در نظر گرفته شد.

کلید واژه ها

نانولوله کربنی چند دیواره؛ چهارچوب ایمیدازول زئولیتی-روی کبالت؛ یون سرب؛ حذف، نانوکامپوزیت.

DOI: 10.30473/ijac.2024.71788.1303